




# Bayesian inference of nuclear incompressibility from proton elliptic flow in central Au+Au collisions at 400 MeV/nucleon

J. M. Wang (汪金梅)<sup>1,2</sup> X. G. Deng (邓先概) <sup>1,2,\*</sup> W. J. Xie (谢文杰)<sup>3</sup> B. A. Li (李宝安) <sup>4,†</sup> and Y. G. Ma (马余刚) <sup>1,2,‡</sup>

<sup>1</sup>Key Laboratory of Nuclear Physics and Ion-beam Application (MOE),  
Institute of Modern Physics, Fudan University, Shanghai 200433, China

<sup>2</sup>Shanghai Research Center for Theoretical Nuclear Physics,  
NSFC and Fudan University, Shanghai 200438, China

<sup>3</sup>Department of Physics, Yuncheng University, Yuncheng 044000, China

<sup>4</sup>Department of Physics and Astronomy, Texas A&M University-Commerce, Texas 75429-3011, USA  
(Dated: June 12, 2024)

The incompressibility  $K$  of symmetric nuclear matter (SNM) is inferred in a Bayesian analysis of proton elliptic flow in mid-central Au + Au collisions at  $E = 400$  MeV/nucleon using a Gaussian process (GP) emulator of the isospin-dependent quantum molecular dynamics (IQMD) model for heavy-ion collisions, with or without considering the momentum dependence of single-nucleon potentials. Consistent but with smaller quantified uncertainties than previous results from forward modeling of the collective flow in heavy-ion collisions using IQMD, considering the momentum dependence of nucleon potentials,  $K = 191.3^{+3.7}_{-6.3}$  MeV at 68% confidence level, indicating a very soft SNM equation of state, is inferred from the combined data of the rapidity and transverse momentum dependence of the proton elliptic flow in the Au+Au collisions considered. Ignoring the momentum dependence of single-nucleon potentials, the extracted value for  $K$  is  $234.7^{+14.6}_{-11.4}$  MeV, in agreement with its fiducial value derived from giant resonance studies.

## I. INTRODUCTION

The equation of state (EoS) of cold symmetric nuclear matter (SNM) is a fundamental relationship between the energy per nucleon  $E/A$  and nucleon density  $\rho$ . At the saturation density  $\rho_0 = 0.16 \text{ fm}^{-3}$  of SNM where  $E/A = -16.0$  MeV and pressure vanishes, the stiffness of SNM EOS is measured by its incompressibility  $K = 9\rho^2 \frac{\partial^2 E/A}{\partial \rho^2} |_{\rho_0}$ . Pinning down precisely the value of  $K$  has been a longstanding and shared goal of both nuclear physics and astrophysics for the last few decades because of its strong impact on many aspects of nuclear structure and reactions as well as properties of neutron stars, mechanisms of supernovae explanations and emissions of gravitational waves from mergers of neutron stars, see, e.g., Refs. [1–20]. Indeed, thanks to the hard work of many people especially over the last 40 years, much progress has been made in constraining  $K$ . In particular, since the pioneering work of Blaizot who determined  $K = (210 \pm 30)$  MeV from analyzing the giant monopole resonance (GMR) energies in  $^{40}\text{Ca}$ ,  $^{90}\text{Zr}$  and  $^{208}\text{Pb}$  [1], extensive theoretical studies and systematic measurements of GMR energies [1, 21–26] have led to the community consensus that the  $K$  is in the range of 220 MeV to 260 MeV [22, 23, 26, 27] or around  $235 \pm 30$  MeV [28, 29] as indicated by the light blue band in Fig. 1.

Another well-known tool for studying the EOS of nu-

clear matter is heavy-ion collisions. In particular, various components of nuclear collective flow (e.g., directed and elliptical flow) as well as yields and spectra of multiple particles (e.g., pions, kaons, photons and dileptons) are useful probes of the EOS albeit with different sensitivities. Information about the EOS is normally extracted by comparing transport model simulations with experimental data in the forward-modeling approach, while in more recent years the data-driven Bayesian inference has become more revealing with quantified uncertainties. In either approach, there are still many interesting issues in narrowing down the remaining uncertainties of various features and parameters of the nuclear EOS using heavy-ion reactions, e.g., Refs. [30–32] for reviews.

The purposes of this work are twofold. Firstly, there is a mild tension between the  $K$  values extracted from analyzing GMR energies and some transport model studies of heavy-ion reactions. For example, as shown by the first point in Fig. 1, analyses of the elliptic flow in Au+Au reactions at beam energies from 0.4 to 1.5 GeV/nucleon from the FOPI collaboration within the Isospin-dependent Quantum Molecular Dynamics (IQMD) model extracted a value of  $K = 190^{+30}_{-30}$  MeV [33]. Moreover, an analysis of the ratio of kaons in Au+Au over C+C systems favors a soft EoS of  $K = 200$  MeV than the hard EoS of  $K = 380$  MeV [34] without giving a quantified uncertainty. Both studies have considered the momentum dependence of isoscalar single-nucleon potentials. The approximately 40 MeV error band of  $K$  from studying GMR and its deviations from the above two  $K$  values from analyzing heavy-ion reactions are still too large for many investigations in both nuclear physics and astrophysics. For example, it has been shown recently that the variation of  $K$  between 220 and 260 MeV leads

\* xiangai.deng@fudan.edu.cn

† Bao-An.Li@Tamuc.edu

‡ mayugang@fudan.edu.cn

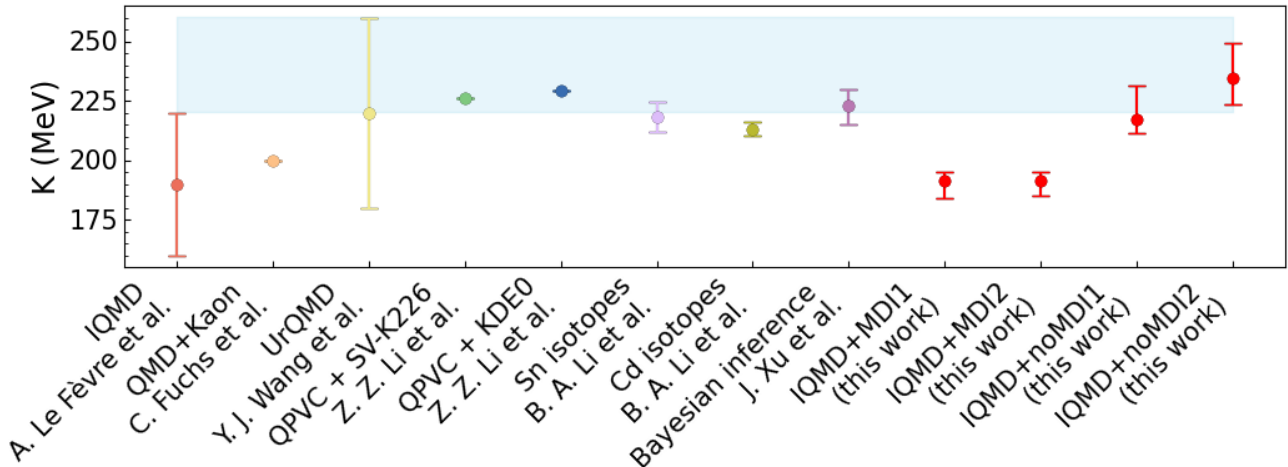


FIG. 1. The light blue band covering  $K = 220 - 260$  MeV is the fiducial range from studying giant resonances [1, 22, 23]. The rest are indicated by the legends from left to right from Refs. [33–38]. The red points with error bars are the results of this work.

to significant changes in the crust-core transition density and pressure in neutron stars [39, 40]. They subsequently affect significantly the radii, tidal polarizabilities, and crustal moments of inertia of canonical neutron stars, hindering the investigations of the very mysterious high-density cores of neutron stars as their properties are often strongly correlated with the value of  $K$ . Thus, a re-extraction of the  $K$  with a quantified uncertainty from heavy-ion collisions in a Bayesian approach will be invaluable.

Secondly, it is known that the momentum dependence of single-nucleon potentials is very important for accurately simulating heavy-ion reactions. However, not all observables are affected equally by it. Thus, sometimes inconsistent conclusions have been drawn about  $K$  based on the analyses of different observables using transport models with or without considering the momentum dependence of single-nucleon potentials. By studying the combined data of rapidity and transverse momentum dependences of proton elliptical flow in mid-central Au+Au reactions at 400 MeV/nucleon, we found incompressibility  $K = 191.3_{-6.3}^{+3.7}$  or  $234.7_{-11.4}^{+14.6}$  MeV at 68% confidence level with or without considering the momentum dependence of single-nucleon potentials, respectively. As shown in Fig. 1, our finding with momentum dependence is consistent with the earlier findings of Refs. [33, 34] but have much smaller errors. Without the momentum dependence, on the other hand, our result is consistent with  $K$ 's fiducial value from GMR studies. We also found that the  $K$  value inferred depends appreciably on whether one includes the transverse momentum dependence of the elliptical flow in the analysis without considering the momentum dependence of nucleon potentials. While we have not studied extensively all observables in a broad beam

energy range yet, our findings reported here are useful for unraveling the physics underlying the compressibility of nuclear matter and eventually pinning down its value precisely.

The rest of this article is organized as follows: in Sec. II, we outline the key ingredients of the IQMD model most relevant for this study. In Sec. III, we recall the key aspects of the Bayesian approach used in this work. In Sec. IV, we present the Gaussian Process (GP) emulator of IQMD, and demonstrate the accuracy of its training and testing. The posterior probability distribution functions (PDFs) of the incompressibility  $K$  as well as the corresponding nuclear interaction parameters from our Bayesian inference in different situations are presented and discussed in Sec. V. In Sec. VI, we summarize our work.

## II. A BRIEF SUMMARY OF THE IQMD MODEL FOR HEAVY-ION REACTIONS

To facilitate comprehension and to be complete, we recall here a few key physics ingredients of IQMD model that are most relevant for this work. This model has been widely employed successfully in studying heavy-ion collisions at low to intermediate beam energies, see, e.g. Refs. [41–51]. The nuclear effective interaction used includes not only a Skyrme term, but also the Yukawa, isospin-asymmetric, and Coulomb terms. Optionally, a momentum-dependent interaction (MDI) term can be turned on or off. More specifically, the EoS, pressure and incompressibility  $K$  for cold SNM can be written as

[41–43, 52–54]:

$$E/A = \frac{\alpha}{2} \frac{\rho}{\rho_0} + \frac{\beta}{\gamma+1} \left( \frac{\rho}{\rho_0} \right)^\gamma + \frac{3}{10m} \left( \frac{3\pi^2 \hbar^3 \rho}{2} \right)^{2/3} + \frac{1}{2} t_4 \frac{\rho}{\rho_0} \int f(\vec{p}) \ln^2 \left[ 1 + t_5 (\vec{p} - \langle \vec{p}' \rangle)^2 \right] d^3 p, \quad (1)$$

$$P = \rho^2 \frac{\partial E/A}{\partial \rho} = \frac{\alpha}{2} \frac{\rho^2}{\rho_0} + \frac{\beta \gamma \rho}{\gamma+1} \left( \frac{\rho}{\rho_0} \right)^\gamma + \frac{1}{5m} \left( \frac{3}{2} \pi^2 \hbar^3 \right)^{\frac{2}{3}} \rho^{\frac{5}{3}} + \frac{t_4}{2} \frac{\rho^2}{\rho_0} \ln^2 (1 + t_5 P_F^2), \quad (2)$$

$$K = 9\rho^2 \frac{\partial^2 E/A}{\partial \rho^2} \Big|_{\rho_0} = -\frac{3}{5m} \left( \frac{3\pi^2 \hbar^3 \rho_0}{2} \right)^{2/3} + \frac{9\beta\gamma(\gamma-1)}{\gamma+1} + \ln(1 + t_5 P_F^2) \frac{6t_4 t_5 P_F^2}{1 + t_5 P_F^2}, \quad (3)$$

where  $\alpha$ ,  $\beta$ ,  $\gamma$ ,  $t_4$  and  $t_5$  are parameters,  $P_F = (3\pi^2 \hbar^3 \rho/2)^{1/3}$  is the nucleon Fermi momentum at density  $\rho$ , and  $f(\vec{p}) = \frac{3}{4\pi P_F^3} \Theta(p_F - p)$ ,  $\Theta$  is the step function. The values of  $t_4 = 1.57$  MeV and  $t_5 = 5 \times 10^{-4} \text{ c}^2/\text{MeV}^2$  are determined by the experimental nucleon optical potential and the isoscalar nucleon effective mass at  $\rho_0$  [41]. The EoS and its characteristics depend only on  $\alpha$ ,  $\beta$ , and  $\gamma$  parameters.

### III. BAYESIAN APPROACH FOR INFERRING EOS PARAMETERS

Bayesian inference is one of the Machine Learning (ML) techniques that have been widely utilized in many fields in recent years. Compared to the traditional  $\chi^2$  fitting in the forward-modeling approach, it has several advantages in determining model parameters with quantified uncertainties, see, e.g. Refs. [38, 55–65]. For completeness, we recall that the Bayes' theorem states that

$$P(\theta | D) = \frac{P(D | \theta) P(\theta)}{P(D)}, \quad (4)$$

where  $P(\theta | D)$  denotes the posterior PDF of model parameter set  $\theta$  given the dataset  $D$ , while  $P(D | \theta)$  is the likelihood for the model with the parameter set  $\theta$  to reproduce the dataset  $D$ . The  $P(\theta)$  is the prior PDF of the parameter set  $\theta$ , and  $P(D)$  serves as the normalization constant. In this study, the  $\theta$  consists of incompressibility  $K$ ,  $\alpha$ ,  $\beta$  and  $\gamma$  constrained by the three SNM saturation conditions at  $\rho_0$  mentioned earlier. Thus, only one parameter is free, and we choose it to be  $K$ . In the Markov Chain Monte Carlo (MCMC) process of our Bayesian analysis, the trial  $K$  value is randomly generated uniformly in the prior range of  $K = 170 \sim 420$  MeV.

Once the incompressibility  $K$  is selected, the corresponding values of  $\alpha$ ,  $\beta$ , and  $\gamma$  are then also obtained from the situation conditions. Additionally, two constraints of  $-1000 < \alpha < 0$  MeV and  $\beta > 0$  MeV are applied to keep nuclear matter stable and remain casual at all densities. Thus, there is a one-to-one correspondence between the incompressibility  $K$  and  $\alpha$ ,  $\beta$ ,  $\gamma$  parameters considering the saturation conditions of SNM at  $\rho_0$  through Eqs. (1)–(3). By inputting a given set of  $\alpha$ ,  $\beta$ , and  $\gamma$  parameters into the IQMD model, theoretical predictions for the reaction observables corresponding to the selected EOS parameter set can be obtained. These predictions will then be used in evaluating the likelihood function as we shall discuss next.

The logarithm of the posterior distribution of parameters is sampled, enabling a transformation of the Bayesian formula [63]:

$$\ln(P(\theta | D)) \propto \ln(P(D | \theta)) + \ln(P(\theta)). \quad (5)$$

The logarithm of the likelihood function is evaluated by using

$$\ln(P(D | \theta)) = -\frac{1}{2} \sum_i \left[ \frac{(y_i^\theta - y_{i,exp})^2}{\sigma_i^2} + \ln(2\pi\sigma_i^2) \right]. \quad (6)$$

In the above,  $\sigma_i = \sqrt{\sigma_{exp}^2 + \sigma_{mod}^2}$  where  $\sigma_{exp}$  and  $\sigma_{mod}$  (evaluated from the emulator) represent respectively the experimental and model errors. The  $y_i^\theta$  and  $y_{i,exp}$  are the model prediction for the observable  $y_i$  and its experimental value, respectively.

### IV. TRAINING AND TESTING A GAUSSIAN PROCESS (GP) EMULATOR OF THE IQMD SIMULATOR

Since calling the computationally expensive IQMD simulator in Bayesian analyses is impractical, its emulator has to be used instead. We use here the popular and well-tested GP emulator. In the following, we provide some details on training and testing the emulator.

In this study, Au + Au collisions at  $E = 400$  MeV/nucleon, and centrality  $0.25 < b_0 < 0.45$  are considered, where  $b_0$  denotes the scaled impact parameter defined as  $b_0 = b/b_{max}$ , with  $b_{max} = 1.15(A_P^{1/3} + A_T^{1/3})$  fm. We use two observables, namely, the rapidity dependence  $-v_2(y_0)$  of proton elliptical flow and its transverse momentum dependence  $-v_2(u_{t0})$ . Here,  $v_2 = \langle \cos 2\phi \rangle = (p_x^2 - p_y^2)/(p_x^2 + p_y^2)$ . The reduced rapidity  $y_0$  is defined as  $y/y_{pro}$ , where  $y = \frac{1}{2} \ln \left( \frac{E+p_z}{E-p_z} \right)$ , and ‘pro’ denotes the incident projectile in the center of mass frame. The transverse (spatial) component  $u_t$  of the 4-velocity  $u$  is given by  $u_t = \beta_t \gamma_c$ . Here, the 3-vector  $\vec{\beta}$  represents the velocity in units of the speed of light, and  $\gamma_c = 1/\sqrt{1-\beta^2}$ .

The unitless transverse momentum  $u_{t0} = u_t/u_{\text{pro}}$  where  $u_{\text{pro}} = \beta_{\text{pro}}\gamma_{\text{pro}}$  is used [66]. To understand the role of the momentum dependence of nucleon potentials, we do comparative studies using two datasets: one group utilizes only the rapidity dependence of proton elliptical flow  $-v_2(y_0)$ , while the other incorporates also its transverse momentum dependence  $-v_2(u_{t0})$ .

The initial value of incompressibility  $K$  is selected by using the Latin hypercube sampling (LHS) [62, 63] to cover its entire prior range uniformly and efficiently, enabling the emulator to efficiently learn and reliably predict reaction observables. In generating the training and testing sets with the IQMD simulator, 220 different  $K$  values form the training set, while an additional 50 different  $K$  values are used for testing purposes. For each incompressibility  $K$ , the IQMD model produces 10,000 events to calculate the respective observables  $-v_2(y_0)$  and  $-v_2(u_{t0})$ , with each event being associated with a randomly selected impact parameter in the range mentioned earlier.

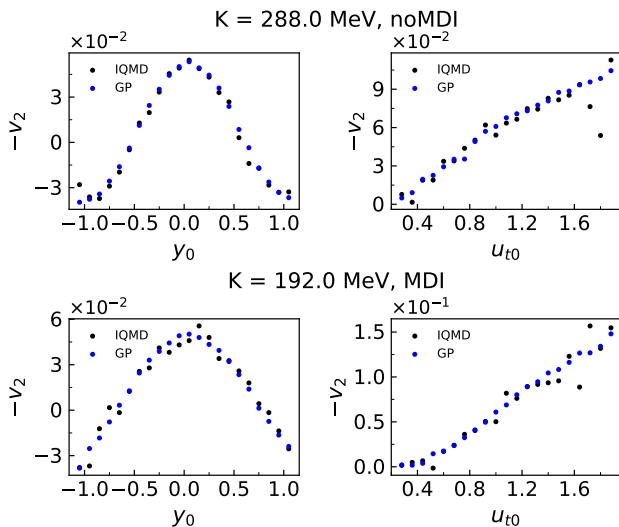


FIG. 2. A comparison between the predictions for  $-v_2(y_0)$  and  $-v_2(u_{t0})$  by the IQMD simulator and the GP emulator for two randomly selected sets of incompressibility  $K$  in the testing dataset. Up: without considering the MDI, down: considering the MDI.

To facilitate effective learning and reliable predictions of observables by the emulator, the commonly employed Radial Basis Function (RBF) is utilized [67]. To assess the emulator's performance on the testing set, shown in Fig. 2 is a visual comparison between the emulator predictions and those generated directly by the IQMD simulator. Clearly, for all the observables in the cases considered, the emulator's performance is satisfactory.

To be more quantitative in evaluating the trustworthiness of the emulator, the mean squared error (MSE) for each observable  $O$  can be used to measure the discrepancy between the emulator predictions  $O_i(\text{GP})$  and the actual outputs  $O_i(\text{IQMD})$  of the IQMD simulator for all

data points ( $i$  runs through all  $n$ -points of each observable shown in Fig. 2) in the testing dataset. The MSE(N) of testing-run  $N$  is defined as [67]:

$$\text{MSE}(N) = \frac{1}{n} \sum_{i=1}^n [O_i(\text{IQMD}) - O_i(\text{GP})]_N^2. \quad (7)$$

Fig. 3(a) and 3(b) show the MSE(N) values for the 50 testing set considered. It is seen that the MSE values are predominantly below 0.00065, signifying the high accuracy of the GP emulator trained for the present study.

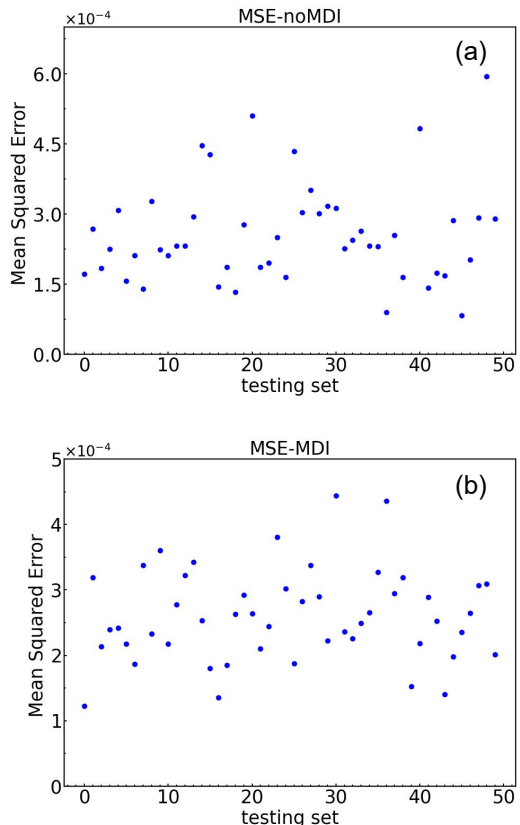


FIG. 3. The MSE(N) between the observables  $-v_2(y_0)$  and  $-v_2(u_{t0})$  predicted by the GP emulator and the IQMD simulator as a function of the testing-run number  $N$ . Up: without considering the MDI, down: considering the MDI.

## V. RESULTS AND DISCUSSIONS OF BAYESIAN ANALYSES

The Affine Invariant MCMC Ensemble sampler algorithm is used to sample the posterior distribution of incompressibility  $K$ . The cumulative mean (running average) diagram from the MCMC sampling is typically employed to assess the convergence status of the sampling process. In our work, each of the five MCMC chains runs independently 3 million steps and throwing away the first 1.2 million burn-in steps.

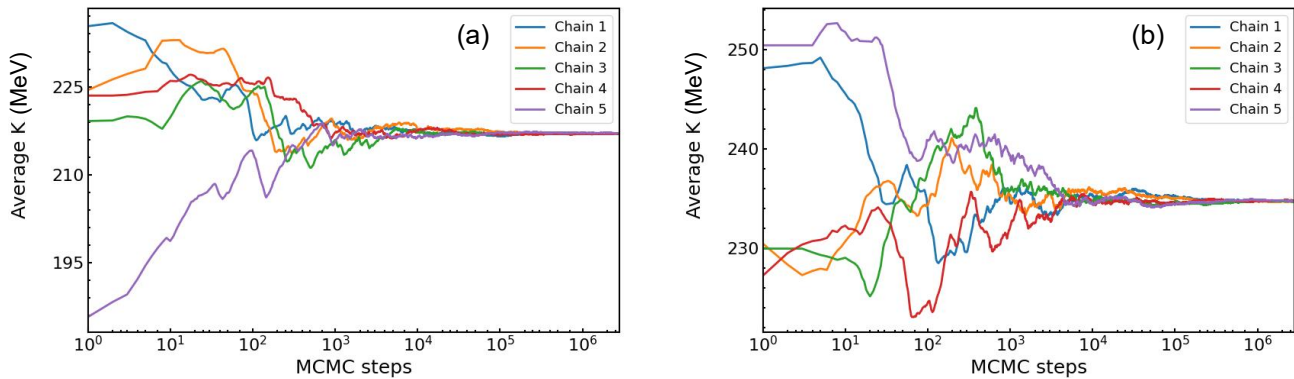


FIG. 4. Without considering the MDI: running averages of the  $K$  as functions of the MCMC steps after 200,000 initial steps in 5 independent chains. Left: observable only  $-v_2(y_0)$ , right: observables  $-v_2(y_0)$  and  $-v_2(u_{t0})$ .

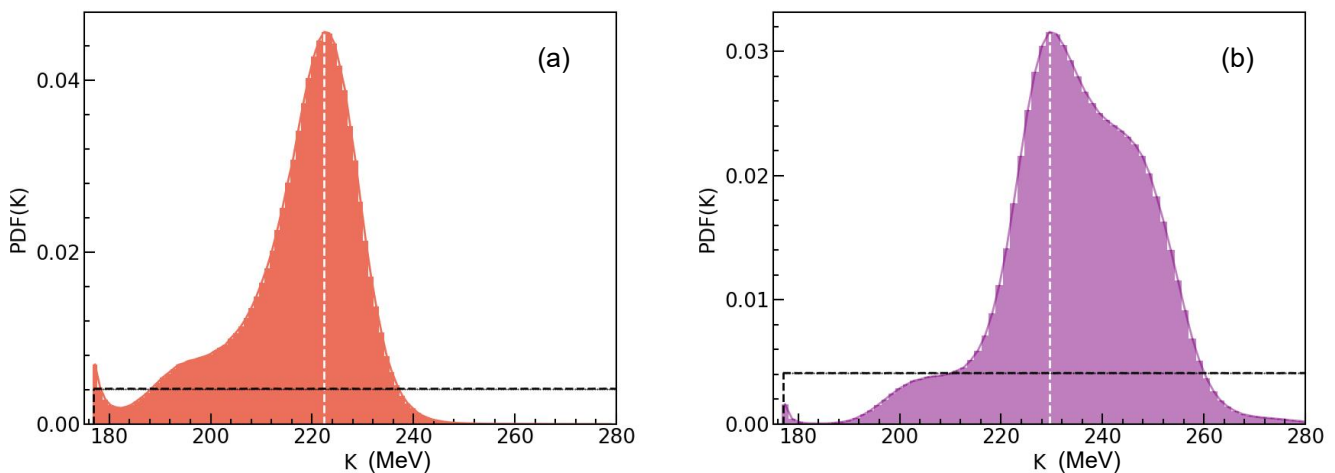


FIG. 5. Without considering the MDI: the posterior PDFs of  $K$ . Left: using only the observable  $-v_2(y_0)$ , right: using the two observables  $-v_2(y_0)$  and  $-v_2(u_{t0})$ .

As mentioned earlier, we shall compare two calculations with or without considering the momentum-dependent interaction (MDI) part of single-nucleon potentials. In both cases, we found that 1 million burn-in steps are sufficient. As an example, shown in Fig. 4(a) and 4(b) are the cumulative mean diagrams of our MCMC sampling without considering the MDI. It is seen that regardless of the initial states, all chains surely converge to the same equilibrium state after about 1 million steps. Moreover, this conclusion is independent of the observables we used. All results presented in the following are obtained by using 3 million steps and throwing away the first 1.2 million burn-in steps.

We first examine the posterior PDFs without considering the MDI. The results obtained from the convergent MCMC chains are illustrated in Fig. 5(a) (using only  $-v_2(y_0)$ ) and 5(b) (using both  $-v_2(y_0)$  and  $-v_2(u_{t0})$ ). We note that the white dashed line corresponds to the most probable value (MPV) of the posterior distribution. The black dashed line represents the prior distribution of

$K$ . The posterior PDF is much narrower than that of the prior one in both cases, indicating that the observables used are very constraining on  $K$ .

It is worth mentioning that here we adopt the highest posterior density (HPD) method to calculate the 68% confidence interval [68] since the posterior distribution of  $K$  normally deviates from a Gaussian distribution as shown in Fig. 5. More specifically, we find from the PDF shown in Fig. 5(a) that the mean value of  $K$  is  $K = 217.1^{+14.2}_{-5.8}$  MeV at 68% confidence interval when only using the observable  $v_2(y_0)$ . On the other hand, from Fig. 5(b), we find  $K = 234.7^{+14.6}_{-11.4}$  MeV when both  $-v_2(y_0)$  and  $-v_2(u_{t0})$  are used. In this case, the mean or MPV of  $K$  is appreciably (by about 17 MeV) larger than that when only the rapidity dependence of elliptical flow data is used. This finding is understandable. The transverse momentum-dependent elliptical flow data,  $v_2(u_{t0})$  indicates that the azimuthal asymmetry of protons increases with  $p_t$ . Generally speaking, to obtain a larger  $v_2$  requires a larger gradient in pressure [69]. It can



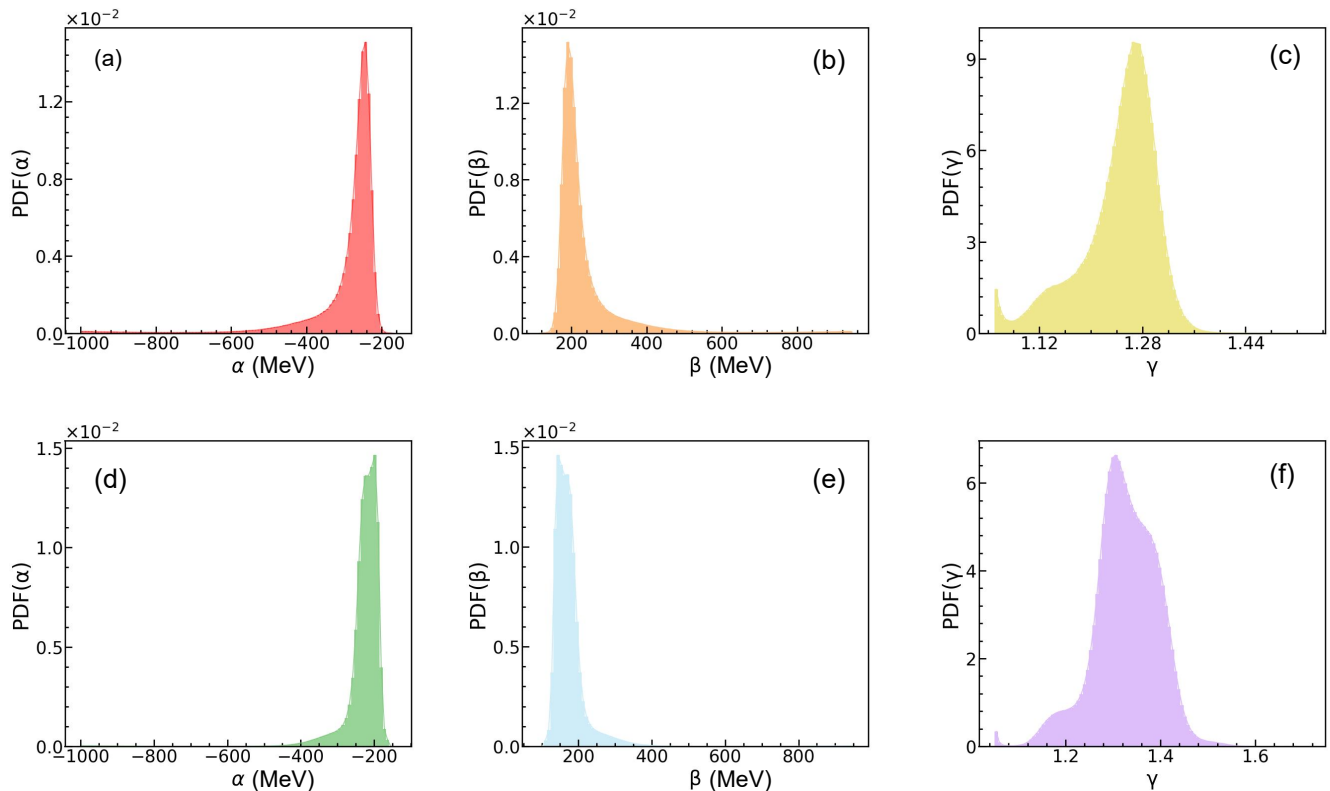


FIG. 6. Without considering the MDI: the posterior PDFs of  $\alpha$ ,  $\beta$  and  $\gamma$ . Up: observable only  $-v_2(y_0)$ , down: observables  $-v_2(y_0)$  and  $-v_2(u_{t0})$ .

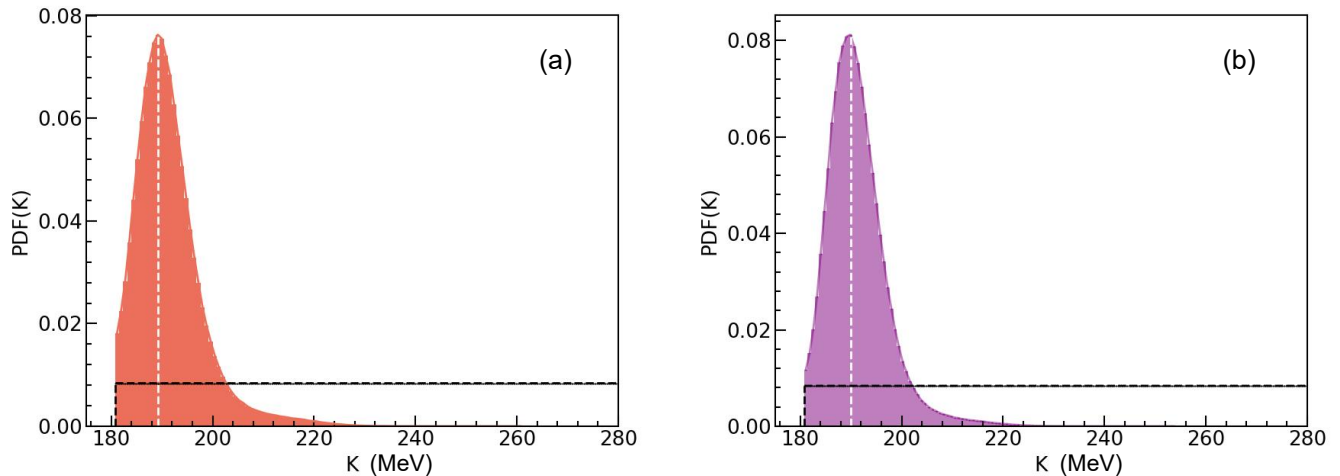


FIG. 7. Considering the MDI: the posterior PDFs of  $K$ . Left: observable only  $-v_2(y_0)$ , right: observables  $-v_2(y_0)$  and  $-v_2(u_{t0})$ .

come from either the density-dependent or momentum-dependent part of the mean-field potential. It is also known that the high- $p_t$  particles are mostly from the high-density region, especially in the earlier stage of the reaction when the system is not thermalized yet [70–73]. The absence of a momentum-dependence potential in the

simulation requires compensation from a stiffer density-dependent EOS to reproduce the large  $v_2$  at high- $p_t$ . Therefore, in the Bayesian analysis without using the MDI, the  $K$  value inferred from the data including transverse momentum dependence of elliptic flow  $-v_2(u_{t0})$  is larger.

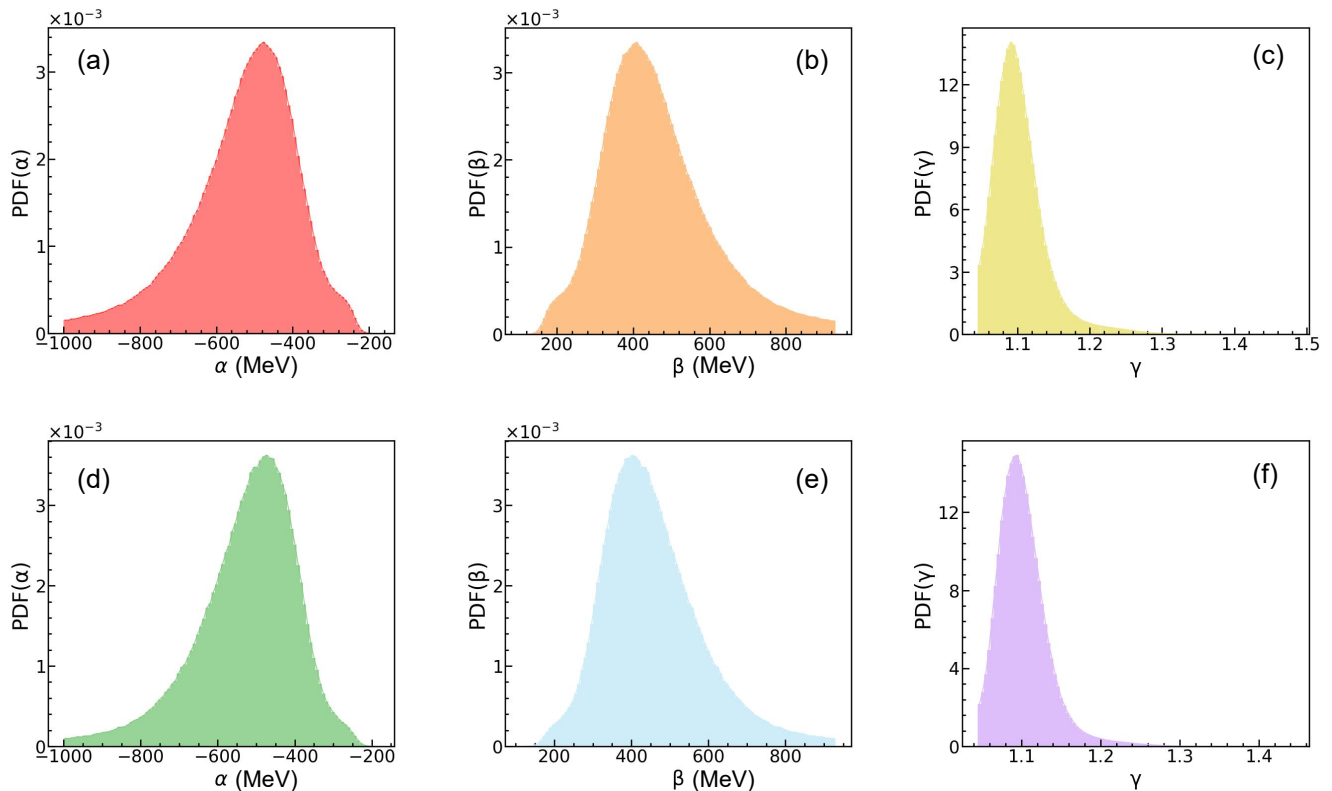


FIG. 8. Considering the MDI: the posterior PDFs of  $\alpha$ ,  $\beta$  and  $\gamma$ . Up: observable only  $-v_2(y_0)$ , down: observables  $-v_2(y_0)$  and  $-v_2(u_{t0})$ .

As discussed earlier, given an incompressibility  $K$  the corresponding parameters  $\alpha$ ,  $\beta$ , and  $\gamma$  can be obtained from the formulas for  $E/A$ ,  $P$  and  $K$  at the saturation point  $\rho_0$ . Here we can readily use the convergent MCMC chains to obtain the posterior PDFs of  $\alpha$ ,  $\beta$  and  $\gamma$ . As shown in Fig. 6(a)–6(f), these PDFs are also much narrower than their prior ranges. These constrained parameters will be useful for testing fundamental interactions, e.g., the Skyrme nuclear effective interactions.

We now turn to the results obtained by using the MDI. We maintain the same prior distributions for incompressibility  $K$  and apply identical constraining conditions as in the previous case. The PDFs for  $K$  are depicted in Fig. 7(a) and 7(b). The corresponding results for  $\alpha$ ,  $\beta$  and  $\gamma$  are illustrated in Fig. 8(a)–8(c) and 8(d)–8(f), respectively. Notably, the mean values of  $K$  are now  $191.4^{+3.5}_{-7.2}$  MeV at 68% confidence level when only the  $-v_2(y_0)$  data is used, and  $191.3^{+3.7}_{-6.3}$  MeV when both the  $-v_2(y_0)$  and  $-v_2(u_{t0})$  observables are used. Interestingly, with the MDI interaction now the  $K$  values inferred are about the same using both datasets. Moreover, they are significantly smaller than the ones inferred earlier in calculations without considering the MDI. These are mainly because the MDI potential is repulsive and becomes stronger with increasing momentum, see, e.g. Ref.[74] for a recent review. It naturally provides a larger

pressure gradient for particles with higher transverse momentum  $p_t$ , without making the density-dependent part of the potential stiffer. Thus, in the case of including the momentum-dependent potential in simulating heavy-ion reactions, regardless of the observable used  $-v_2(y_0)$  alone or including the  $-v_2(u_{t0})$ , the required  $K$  value to reproduce the data remains more or less the same. It is also well-known that the MDI reduces the necessary  $K$  to reproduce flow data. Our results are consistent with the earlier findings, see, e.g. Refs. [33, 34, 75–77].

As mentioned earlier, one main advantage of performing Bayesian inference is the ability to obtain quantified uncertainties of the model parameters. Such information regarding the incompressibility  $K$  in this study is summarized in Table I. Our results indicate that regardless of the observables used in the analyses with considering the MDI, the derived  $K$  is significantly smaller than its fiducial value from studying GMR energies as shown in Fig. 1. Moreover, the width of the 68% confidence band of  $K$  with the MDI is significantly narrower than that without considering the MDI. This is partially because the strength and shape of the MDI in the IQMD model are fixed as discussed earlier. Also, it is known that the maximum density reached with the MDI is less than that reached otherwise, see, e.g. Refs. [75, 78–80]. Together they make the necessary  $K$  to reproduce the data less uncertain.

TABLE I. The mean (at 68% confidence level) and the most probable value of the incompressibility  $K$  (MeV) inferred with and without considering the momentum-dependent interaction.

	noMDI		MDI	
Observables:	$-v_2(y_0)$	$-v_2(y_0), -v_2(u_{t0})$	$-v_2(y_0)$	$-v_2(y_0), -v_2(u_{t0})$
$K$ Mean	$217.1^{+14.2}_{-5.8}$	$234.7^{+14.6}_{-11.4}$	$191.4^{+3.5}_{-7.2}$	$191.3^{+3.7}_{-6.3}$
$K$ MPV	222.4	229.5	189.2	189.9

## VI. SUMMARY

In summary, within a Bayesian statistical framework using a Gaussian Process emulator for the IQMD simulator we inferred the incompressibility  $K$  of SNM from the proton elliptic flow data in mid-central Au+Au reactions at 400 MeV/nucleon from the FOPI collaboration. Compared to previous works mostly based on transport model simulations in the forward-modeling approach, Bayesian analyses enable us to infer the underlying transport model parameters with quantified uncertainties. In particular, we inferred an incompressibility  $K = 191.3^{+3.7}_{-6.3}$  MeV at 68% confidence level from the combined data of rapidity and transverse momentum dependence of the proton elliptic flow in analyses considering the momentum dependence of single-nucleon potentials. It is consistent with the results from previous analyses of the same data using forward modeling but with much smaller errors. However, it is significantly smaller than its fiducial value derived from giant resonance studies over the last 40 years. This tension remains an interesting issue to be resolved.

We also found that the MDI effects on extracting the incompressibility  $K$  from heavy-ion reactions depend on what observables are included in the dataset. In particular, the transverse momentum dependence of elliptical flow  $v_2(p_t)$  reflects the pressure gradients experienced by particles from low to high-density regions during the whole reaction. Without including the MDI in transport model simulations, reproducing the  $v_2(p_t)$  data, especially at high- $p_t$ , requires the density-dependent part of the EOS to be stiffer than what is necessary to reproduce only the rapidity dependence of elliptical flow which

is dominated by thermalized nucleons.

Because GMR is a collective motion of nucleons at low densities while the flow is a collective motion of nucleons at high densities and some with high momenta, it is not surprising that the  $K$  values extracted from studying GMR energies may be different from its values extracted from investigating various flow observables in heavy-ion reactions. Indeed, without considering the MDI,  $K = 217.1^{+14.2}_{-5.8}$  MeV or  $K = 234.7^{+14.6}_{-11.4}$  MeV were inferred using only the  $-v_2(y_0)$  or using both the  $-v_2(y_0)$  and  $-v_2(u_{t0})$ , respectively. These are in good agreement with the fiducial value of  $K$  within its still relatively larger error band of about 40 MeV as shown in Fig. 1.

## ACKNOWLEDGMENTS

We would like to thank Prof. Kai Zhou for useful communications. Wang, Deng and Ma were supported in part by the National Natural Science Foundation of China under contract Nos. 12147101, 12347149, 11890714, and 11925502, and the Strategic Priority Research Program of CAS under Grant No. XDB34000000. XIE was supported in part by the Shanxi Provincial Foundation for Returned Overseas Scholars under Grant No. 20220037, the Natural Science Foundation of Shanxi Province under Grant No. 20210302123085, and the discipline construction project of Yuncheng university. B.A. Li acknowledges support by the U.S. Department of Energy, Office of Science, under Award No. DE-SC0013702, and the CUSTIPEN (China-U.S. Theory Institute for Physics with Exotic Nuclei) under U.S. Department of Energy Award No. DE-SC0009971.

- 
- [1] J. P. Blaizot, *Phys. Rep.* **64**, 171 (1980).
  - [2] P. Möller, W. D. Myers, H. Sagawa *et al.*, *Phys. Rev. Lett.* **108**, 052501 (2012).
  - [3] P. Senger *et al.* (CBM Collaboration), *Phys. Scr.* **96**, 054002 (2021).
  - [4] G. F. Burgio, H.-J. Schulze, I. Vidaña *et al.*, *Prog. Part. Nucl. Phys.* **120**, 103879 (2021).
  - [5] J. B. Wei, J. J. Lu, G. F. Burgio *et al.*, *Eur. Phys. J. A* **56**, 63 (2020).
  - [6] G. F. Burgio, I. Vidaña, *Universe* **6**, 199 (2020).
  - [7] S. Balberg, I. Lichtenstadt, G. B. Cook, *Astrophys. J. Suppl.* **121**, 515 (1999).
  - [8] M. Oertel, F. Gulminelli, C. Providência *et al.*, *Eur. Phys. J. A* **52**, 50 (2016).
  - [9] D. Chatterjee, I. Vidaña, *Eur. Phys. J. A* **52**, 29 (2016).
  - [10] D. Gerstung, N. Kaiser, W. Weise, *Eur. Phys. J. A* **56**, 175 (2020).
  - [11] R. Wang, Y. G. Ma, R. Wada *et al.*, *Phys. Rev. Res.* **2**,



- 043202 (2020).
- [12] Y. G. Ma, L. G. Pang, R. Wang *et al.*, *Chinese Phys. Lett.* **40**, 122101 (2023).
- [13] L. G. Pang, X. N. Wang, *Nucl. Sci. Tech.* **34**, 194 (2023).
- [14] X. G. Deng, D. Q. Fang, Y. G. Ma, *Prog. Part. Nucl. Phys.* **136**, 104095 (2024).
- [15] J. F. Xu, L. Cui, Z. Y. Lu *et al.*, *Nucl. Sci. Tech.* **34**, 171 (2023).
- [16] J. F. Xu, C. J. Xia, Z. Y. Lu *et al.*, *Nucl. Sci. Tech.* **33**, 143 (2022).
- [17] N. B. Zhang, B. A. Li, *Nucl. Sci. Tech.* **29**, 178 (2018).
- [18] J. Y. Xu, Z. Z. Li, B. H. Sun *et al.*, *Phys. Lett. B* **833**, 137333 (2022).
- [19] H. Shen, F. Ji, J. N. Hu *et al.*, *Astrophys. J.* **891**, 148 (2020).
- [20] J. M. Lattimer, *Annu. Rev. Nucl. Part. Sci.* **71**, 433 (2021).
- [21] D. H. Youngblood, H. L. Clark, Y.-W. Lui, *Phys. Rev. Lett.* **82**, 691 (1999).
- [22] U. Garg, G. Colò, *Prog. Part. Nucl. Phys.* **101**, 55 (2018).
- [23] X. Roca-Maza, N. Paar, *Prog. Part. Nucl. Phys.* **101**, 96 (2018).
- [24] J. Piekarewicz, *J. Phys. G* **37**, 064038 (2010).
- [25] J. R. Stone, N. J. Stone, S. A. Moszkowski, *Phys. Rev. C* **89**, 044316 (2014).
- [26] G. Colò, U. Garg, H. Sagawa, *Eur. Phys. J. A* **50**, 26 (2014).
- [27] S. Shlomo, V.M. Kolomietz, G. Colò, *Eur. Phys. J. A* **30**, 23 (2016).
- [28] E. Khan, J. Margueron, I. Vidaña, *Phys. Rev. Lett.* **109**, 092501 (2012).
- [29] J. Margueron, R. Hoffmann Casali, F. Gulminelli, *Phys. Rev. C* **97**, 025805 (2018).
- [30] B. A. Li, L. W. Chen, C. M. Ko, *Phys. Rep.* **464**, 113 (2008).
- [31] H. Wolter *et al.* (TMEP Collaboration), *Prog. Part. Nucl. Phys.* **125**, 103962 (2022).
- [32] A. Sorensen, K. Agarwal, K. W. Brown *et al.*, *Prog. Part. Nucl. Phys.* **134**, 104080 (2024).
- [33] A. Le Fèvre, Y. Leifels, W. Reisdorf *et al.*, *Nucl. Phys. A* **945**, 112 (2016).
- [34] C. Fuchs, *Prog. Part. Nucl. Phys.* **53**, 113 (2004).
- [35] Y. J. Wang, C. C. Guo, Q. F. Li *et al.*, *Phys. Lett. B* **778**, 207 (2018).
- [36] Z. Z. Li, Y. F. Niu, G. Colò, *Phys. Rev. Lett.* **131**, 082501 (2023).
- [37] B. A. Li, W. J. Xie, *Phys. Rev. C* **104**, 034610 (2021).
- [38] J. Xu, Z. Zhang, B. A. Li, *Phys. Rev. C* **104**, 054324 (2021).
- [39] B. A. Li, M. Magno, *Phys. Rev. C* **102**, 045807 (2020).
- [40] J. Richter, B. A. Li, *Phys. Rev. C* **108**, 055803 (2023).
- [41] J. Aichelin, A. Rosenhauer, G. Peilert *et al.*, *Phys. Rev. Lett.* **58**, 1926 (1987).
- [42] J. Aichelin, *Phys. Rep.* **202**, 233 (1991).
- [43] C. Hartnack, R. K. Puri, J. Aichelin *et al.*, *Eur. Phys. J. A* **1**, 151 (1988).
- [44] Y. X. Zhang, N. Wang, Q. F. Li *et al.*, *Front. Phys.* **15**, 54301 (2020).
- [45] Y. X. Zhang, Y. J. Wang, M. Colonna *et al.*, *Phys. Rev. C* **97**, 034625 (2018).
- [46] S. N. Wei, Z. Q. Feng, *Nucl. Sci. Tech.* **35**, 15 (2024).
- [47] F. Y. Wang, J. P. Yang, X. Chen *et al.*, *Nucl. Sci. Tech.* **34**, 94 (2023).
- [48] K. Xiao, P. C. Li, Y. J. Wang *et al.*, *Nucl. Sci. Tech.* **34**, 62 (2023).
- [49] R. S. Wang, L. Ou, Z. G. Xiao, *Nucl. Sci. Tech.* **33**, 92 (2023).
- [50] L. Li, F. Y. Wang, Y. X. Zhang, *Nucl. Sci. Tech.* **33**, 58 (2023).
- [51] C. Liu, X. G. Deng, Y. G. Ma, *Nucl. Sci. Tech.* **33**, 52 (2023).
- [52] L. P. Csernai, G. Fai, C. Gale *et al.*, *Phys. Rev. C* **46**, 736 (1992).
- [53] G. Giuliani, H. Zheng, A. Bonasera, *Prog. Part. Nucl. Phys.* **76**, 116 (2014).
- [54] Y. K. Vermani, S. Goyal, R. K. Puri, *Phys. Rev. C* **79**, 064613 (2009).
- [55] S. Pratt, E. Sangaline, P. Sorensen *et al.*, *Phys. Rev. Lett.* **114**, 202301 (2015).
- [56] J. Novak, K. Novak, S. Pratt *et al.*, *Phys. Rev. C* **89**, 034917 (2014).
- [57] J. E. Bernhard, P. W. Marcy, C. E. Coleman-Smith *et al.*, *Phys. Rev. C* **91**, 054910 (2015).
- [58] J. E. Bernhard, J. S. Moreland, S. A. Bass, *Nature Phys.* **15**, 1113 (2019).
- [59] W. B. He, Q. F. Li, Y. G. Ma *et al.*, *Sci. China Phys. Mech. Astron.* **66**, 282001 (2023).
- [60] W. B. He, Y. G. Ma, L. G. Pang *et al.*, *Nucl. Sci. Tech.* **34**, 88 (2023).
- [61] K. Zhou, L. X. Wang, L. G. Pang *et al.*, *Prog. Part. Nucl. Phys.* **135**, 104084 (2024).
- [62] B. A. Li, W. J. Xie, *Nucl. Phys. A* **1039**, 122726 (2023).
- [63] M. O. Kuttan, J. Steinheimer, K. Zhou *et al.*, *Phys. Rev. Lett.* **131**, 202303 (2023).
- [64] P. Morfouace, C. Y. Tsang, Y. Zhang *et al.*, *Phys. Lett. B* **799**, 135045 (2019).
- [65] N. K. Patra, S. M. A. Imam, B. K. Agrawal *et al.*, *Phys. Rev. D* **106**, 043024 (2022).
- [66] W. Reisdorf *et al.* (FOPI Collaboration), *Nucl. Phys. A* **876**, 1 (2012).
- [67] C. E. Rasmussen, C. K. I. Williams, MA: MIT press <http://gaussianprocess.org/gpml/> (2006).
- [68] N. Turkkkan, T. Pham-Gia, *J. Stat. Comput. Sim.* **44**, 243 (1993).
- [69] J.-Y. Ollitrault, *Nucl. Phys. A* **638**, 195c (1998).
- [70] G. F. Bertsch, S. Das Gupta, *Phys. Rep.* **160**, 189 (1988).
- [71] W. Cassing, V. Metag, U. Mosel *et al.*, *Phys. Rep.* **188**, 363 (1990).
- [72] S. A. Bass *et al.*, *Prog. Part. Nucl. Phys.* **41**, 255 (1998).
- [73] P. Danielewicz, R. Lacey, W. G. Lynch, *Science* **298**, 1592 (2002).
- [74] B. A. Li, B. J. Cai, L. W. Chen *et al.*, *Prog. Part. Nucl. Phys.* **99**, 29 (2018).
- [75] C. Gale, G. Bertsch, S. Das Gupta, *Phys. Rev. C* **35**, 1666 (1987).
- [76] P. Danielewicz, *Nucl. Phys. A* **673**, 375 (2000).
- [77] P. Danielewicz, Roy A. Lacey, P.-B. Gossiaux *et al.*, *Phys. Rev. Lett.* **81**, 2438 (1998).
- [78] G. F. Bertsch, G. E. Brown, V. Koch *et al.*, *Nucl. Phys. A* **490**, 745 (1988).
- [79] O. Buss *et al.*, *Phys. Rep.* **512**, 1 (2012).
- [80] B. A. Li, C. B. Das, S. Das Gupta *et al.*, *Nucl. Phys. A* **735**, 563 (2004).